



**Optical nanothermometer based on the calibration of the Stokes and upconverted green emissions of Er<sup>3+</sup> ions in Y<sub>3</sub>Ga<sub>5</sub>O<sub>12</sub> nano-garnet**

Journal:	<i>RSC Advances</i>
Manuscript ID:	RA-ART-09-2014-011565
Article Type:	Paper
Date Submitted by the Author:	30-Sep-2014
Complete List of Authors:	León Luis, Sergio; Universidad de La Laguna, Departamento de Física Monteseuro, Virginia; Universidad de la Laguna, Departamento de Física Rodriguez-Mendoza, Ulises; Universidad de La Laguna, Department of Fundamental and Experimental Physics Rathaiah, Mamilla; Yogi Vemana University, Department of Physics Venkatramu, Vemula; Yogi Vemana University, Department of Physics Lozano-Gorriñ, Antonio; Universidad de La Laguna, Valiente, Rafael; University of Cantabria, Applied Physics Munoj, A; Univesidad de La Laguna, Depertmeneto de Fisica Fundamenta III Lavín-della-Ventura, Victor; Universidad de La Laguna,

## ARTICLE

## Optical nanothermometer based on the calibration of the Stokes and upconverted green emissions of Er<sup>3+</sup> ions in Y<sub>3</sub>Ga<sub>5</sub>O<sub>12</sub> nano-garnet

Cite this: DOI: 10.1039/x0xx00000x

Received 00th January 2012,  
Accepted 00th January 2012

DOI: 10.1039/x0xx00000x

[www.rsc.org/](http://www.rsc.org/)

S. F. León-Luis<sup>a,\*</sup>, V. Montenegro<sup>a</sup>, U. R. Rodríguez-Mendoza<sup>a,b</sup>, M. Rathaiah<sup>c</sup>, V. Venkatramu<sup>c</sup>, A. D. Lozano-Gorrín<sup>a</sup>, R. Valiente<sup>d</sup>, A. Muñoz<sup>a,b</sup>, V. Lavín<sup>a,e</sup>.

The temperature-dependent green luminescence of Y<sub>3</sub>Ga<sub>5</sub>O<sub>12</sub> nano-garnets doped with different concentrations of Er<sup>3+</sup> ions has been measured from 300 to 850 K and, in more detail, in the biological range from 292 to 335 K. The green emissions were obtained exciting both under 488 nm blue or 800 nm near-infrared laser radiations. Both excitations give rise to bright green luminescence that can be seen by the naked eyes, and which can be associated either with Stokes processes, i.e. multiphonon relaxations followed by green spontaneous emission, in the former case or with infrared-to-visible upconversion processes in the latter one. The temperature-induced changes in the Er<sup>3+</sup> green emissions have been calibrated for both excitations and results point to a strong dependence on the concentration of optically active Er<sup>3+</sup> ions. The maximum value of the thermal sensitivity, 64 × 10<sup>-4</sup> K<sup>-1</sup> at 547 K, has been obtained for the nano-garnets doped with the lowest concentration of Er<sup>3+</sup> ions, being one of the highest values found in the literature. These results allow concluding that a relatively low concentration of optically active ions is advisable and the changes induced by temperature on the green emissions are independent of the laser excitation radiation used, necessary to calibrate the temperature of the immediate environment of the Er<sup>3+</sup>-doped Y<sub>3</sub>Ga<sub>5</sub>O<sub>12</sub> nano-garnets.

### A. Introduction.

Temperature is the key variable that guarantees a satisfactory result in many industrial processes. Therefore, the development of devices that allow the correct monitoring of the temperature has been a hot topic in the last decades<sup>1</sup>. Nowadays, temperature devices must be fast and accurate but, furthermore, the nanotechnology era requires that they should have extremely low dimensions. All these facts make the micro/nano thermometry one of the most active research areas<sup>2</sup>.

From the point of view of the industrial applicability, nanothermometers are used in photonics integrated circuits to control the temperature, since light can produce thermal heating in the optical components. They can also be placed where the current could generate "hot spots" in the electronics circuits due to the Joule's effect<sup>3</sup>. On the other side, medicine is possibly the research area in which the nanothermometers have found higher impact and applicability in the last decade, since the sizes of the nanoparticles are similar to those of the majority of biological microorganisms (cell, bacteria, etc.). Moreover, nanoparticles can also be used to eliminate the presence of cancer cells in an infected tissue through a local heating process by the direct absorption of a laser radiation or using other nanoparticles that produce heat when they are excited at

a suitable laser radiation wavelength. In this "in vivo" experiments, the nanothermometers are employed to perform a thermal mapping of the irradiated tissue since an accurate temperature control is required<sup>4,5</sup>.

It is worth noting that the main benefit of the nanothermometers, i.e. their nanometric sizes, is also their main drawback, since they cannot be physically connected by wires to a measuring device, as it happens with the thermocouples. Thus an "in-situ", indirect measurement of the local temperature is necessary to solve this problem: the nano-sensors used should be materials that, under lamp or laser excitations, emit light and their temperature dependence must be calibrated using the changes of one or more measurable parameters, such as the lifetimes of the emitting levels, the bandwidth of the emissions, the intensities, the spectral positions, their polarization, etc., with the local temperature around the nano-sensors. Using one of these factors, the luminescence of quantum dots and colloidal nano-crystals have been proposed and calibrated for their use as local temperature probe<sup>6</sup>. However, the high toxicity of these materials limits their applicability in biomedicine. In contrast, rare earth (RE<sup>3+</sup>) doped inorganic nanoparticles have the advantages of better biologic compatibility and smaller toxicity, together with a large emission spectra in the UV-VIS-NIR optical range. All these features make the RE<sup>3+</sup>-doped nanoparticles one of the best options to develop new optical temperature sensors<sup>7</sup>.

Although different parameters can be used to calibrate the temperature dependence of the luminescence, the most widely used technique is the change of the intensity of the luminescence with temperature, known as the fluorescence intensity ratio, which associates the changes of the relative emission intensities of two thermally coupled emitting levels with the local temperature of the nano-sensor's surroundings<sup>8</sup>. However, it should be noted that not all the thermalized levels can be used, and some practical general requirements must be fulfilled: a) the energy gap between the thermalized levels must be large enough to avoid strong overlapping of the two emissions ( $> 200 \text{ cm}^{-1}$ ), and short enough ( $< 2000 \text{ cm}^{-1}$ ) to allow the upper level to have a minimum population of optically active ions in the temperature range of interest, and b) the radiative probabilities of the thermalized levels must be high enough to show large emission intensities<sup>9,10</sup>.

There are some  $\text{RE}^{3+}$  ions that match these conditions to a greater or lesser extent, i.e.  $\text{Pr}^{3+}$ ,  $\text{Nd}^{3+}$ ,  $\text{Sm}^{3+}$ ,  $\text{Eu}^{3+}$  and  $\text{Er}^{3+}$ <sup>9,10</sup>. However,  $\text{Er}^{3+}$  and  $\text{Nd}^{3+}$  ions have a special feature that distinguishes them from other  $\text{RE}^{3+}$  ions: their visible luminescence can be obtained by infrared-to-visible energy upconversion processes without co-doping with  $\text{Yb}^{3+}$  ions using near infrared laser radiations<sup>11-13</sup>. The possibility to obtain the same luminescence using different excitation wavelengths increases the number of applications for which these sensors can be employed. This point is particularly interesting in medical applications because the skin is much more transparent to infrared laser radiation than the visible one<sup>14</sup>.

On the other side, and in order to find better hosts matrices, the efforts have been focused on calibrating crystalline nano-garnets due to their high emission efficiencies and low-energy phonons. In this respect, the favorable features of the oxide garnet crystals such as high transparency from the UV to the mid-IR range, good chemical stability, high thermal conductivity, and the relative low-energy phonons, make them one of the most important families of matrices to be doped with  $\text{RE}^{3+}$  ions<sup>15</sup>. In fact, in the last decades, a great scientific effort has been made in the development and optimization of  $\text{Nd}^{3+}$  and  $\text{Er}^{3+}$  garnet crystals (YAG, GGG,...) as laser active medium<sup>16,17</sup>. As part of this research, the thermal effect on the luminescence has been observed and evaluated as a technique to estimate the quantum efficiency of these active media. This confirms that the luminescence of  $\text{Er}^{3+}$  ions in this host family is sensitive to temperature changes and, therefore, it can be calibrated and used as temperature probe<sup>18</sup>. However, and within to our knowledge, its emission temperature dependence has never been studied or applied in an optical temperature sensor<sup>19</sup>.

The aim of this paper is to calibrate the green emissions of  $\text{Er}^{3+}$  ions in  $\text{Y}_3\text{Ga}_5\text{O}_{12}$  (YGG) nano-garnets to propose them as local probes for temperature measurements in the range from 300 K up to 800 K, i. e. the working range of the majority of industrial processes. Moreover, a careful calibration for the biological range (292-335 K) has been also carried out. Since the concentration of optically active ions affects the sensitivity of the optical sensor in bulk matrices<sup>20</sup>, this work will also explore whether this effect also occurs in the YGG nano-garnets. Finally, the behavior of the green emissions with temperature is analyzed as a function of the exciting laser wavelength by choosing a blue laser radiation at 488 nm and a near-infrared (NIR) laser at 800 nm.

## B. Method.

### B.A. Experimental.

The nano-garnet powders, with chemical formula  $\text{Y}_{3(1-x)}\text{Er}_{3x}\text{Ga}_5\text{O}_{12}$  ( $x=0.001, 0.01$  and  $0.05$ ), were prepared by the conventional citric acid sol-gel Pechini method, and labeled

as YGG01Er, YGG1Er and YGG5Er, respectively<sup>19</sup>. The nanocrystalline powder has been obtained in the form of agglomerated nanocrystals with different shapes and sizes ranging from 40 to 60 nm. The existence of aggregated particles has been ascribed to the bridging of adjacent particles through the hydrogen bonding of water and the significant capillary action generated during the drying process in the precursors<sup>19</sup>. However, X-ray diffraction measurements reveal well-defined Bragg reflections of the nanocrystalline powder samples, indicating that the material under study is well-crystallized in a single phase of cubic garnet crystalline structure (space group Ia-3d,  $N^\circ$  230), although the lattice parameter is 6% larger than in YGG bulk crystal. The garnet crystalline structure can be described as a network of  $\text{GaO}_6$  octahedra ( $S_6$ ) and  $\text{GaO}_4$  tetrahedra ( $S_4$ ) linked by shared oxygen ions at the corners of the polyhedra. These polyhedra are arranged in chains along the three crystallographic directions and form dodecahedral cavities ( $D_2$ ) which are occupied by the  $\text{Y}^{3+}$  ions. In this position, and due to the ionic size considerations, the  $\text{RE}^{3+}$  ions are expected to predominantly enter in the structure replacing the  $\text{Y}^{3+}$  ions. Moreover, the vibrational modes and the optical properties of the  $\text{RE}^{3+}$  ions in these nano-garnets are also quite similar to those found in the YGG bulk crystal<sup>19-21</sup>.

The visible and NIR diffuse reflectance spectrum in the range from 200 to 1800 nm was measured using a spectrophotometer with an integrating sphere (Agilent Cary 5000). In order to carry out the luminescence experiments, the  $\text{Er}^{3+}$ -doped YGG nano-garnets were pressed at 0.1 GPa to obtain circular pellets of 1.3 mm of diameter and 0.2 mm of thickness, which are placed at the center of a tubular electric furnace, as shown in **Figure 1**. The furnace's temperature was increased to a rate of 1 K/min, while the pellet temperature was controlled carefully with a type K thermocouple in contact with it and connected to a voltmeter (Fluke Calibrator 714) with a resolution of  $\pm 0.7$  K. Two laser wavelengths were used to obtain the green emissions of  $\text{Er}^{3+}$  ions: the 488 nm line of a 10 W  $\text{Ar}^{3+}$  laser (Spectra Physics 2060-10 Beamlock) and the 800 nm radiation of a tunable Ti:Sapphire laser (Spectra-Physics 3900S) pumped by a 532 nm laser (Spectra Physics Millennia 15SJSPG). Two convex lenses located just outside the furnace collimated and focalized the emission of  $\text{Er}^{3+}$  ions in an optical fiber coupled to a 0.3 m single grating spectrometer (Andor SR-3031-B), equipped with a cooled CCD detector (Newton DU920N) with a resolution of 0.7 nm ( $\sim 25 \text{ cm}^{-1}$ ) and an integration time of 1 s. A small laser mirror located between the lenses was used to introduce the laser pump in the furnace (see **Figure 1**).

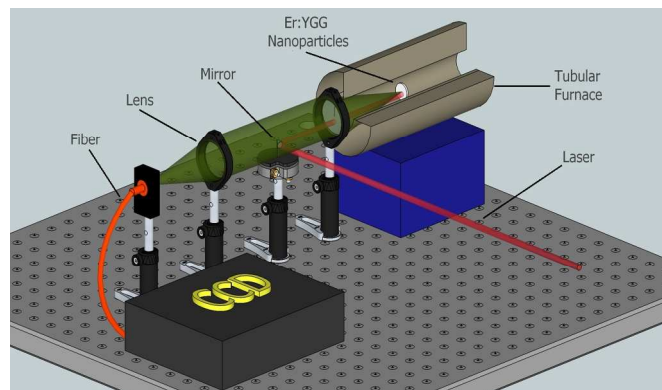


**Figure 1.** Experimental setup made for the temperature-dependent luminescence measurements. The small mirror is used to introduce the laser beam in the furnace.

The laser pump power at both excitation wavelengths was kept as low as possible in order not to heat the sample. The spectra were corrected from the instrument response. All experiments have been performed without dissolving the nanoparticles in any liquid.

### B.B. The fluorescence intensity ratio technique and the optical sensor calibration.

The fluorescence intensity ratio technique has been used to calibrate the  $\text{Er}^{3+}:\text{YGG}$  optical temperature sensor. The theoretical expression used to fit the experimental data can be easily obtained assuming a Boltzmann distribution for a system in thermal equilibrium and from the definition, given by the atomic spectroscopy, of the emission intensity of an electronic  $2S+1L_J$  level.

In a  $\text{RE}^{3+}$ -doped matrix, the relative population of ions between the  $k$ -ground state, and an excited  $i$ -th level at a temperature  $T$  is ruled by the Boltzmann distribution<sup>22</sup>

$$\frac{N_i}{N_k} = \frac{g_i}{g_k} e^{-\frac{E_{ik}}{K_B T}} \quad (1)$$

where  $N$  and  $g$  are the population and the degeneracy ( $2J+1$ ) of each level;  $K_B$  is the Boltzmann constant; and  $E_{ik}$  is the energy gap between the levels involved.

On the other side, the emission intensity of a  $\text{RE}^{3+}$  ion in an excited level  $i$  that decays to ground state level  $k$  is proportional to the ion population in that level  $N_i$ , the spontaneous radiative emission rate  $A_i$ , the branching ratio of the transition studied  $\beta_{ik}$ , and the photon energy emitted  $h\nu_{ik}$ ,

$$I_{ik} \propto N_i \beta_{ik} A_i h\nu_{ik} \quad (2)$$

All these parameters depend on the matrix selected, which explains the differences of emission characteristics between matrices with different chemical compositions.

The last two expressions allow establishing a relationship between the intensity ratio  $R$  of two closed-energy thermalized levels  $i$  and  $j$ , and the temperature of a  $\text{RE}^{3+}$ -doped matrix in thermal equilibrium with its environment as follows<sup>22</sup>,

$$\begin{aligned} R_{Theor} &= \frac{I_{ik}}{I_{jk}} = \frac{C_i(\nu) N_i \beta_{ik} A_i h\nu_{ik}}{C_j(\nu) N_j \beta_{jk} A_j h\nu_{jk}} \\ &= \frac{g_i}{g_j} \frac{C_i(\nu) \beta_{ik} A_i h\nu_{ik}}{C_j(\nu) \beta_{jk} A_j h\nu_{jk}} e^{-\frac{E_{ij}}{K_B T}} \end{aligned} \quad (3)$$

where the populations ratio has been substituted by the Boltzmann distribution. In this expression, the instrument response  $c(\nu)$  has been included, although it can be considered equal to unity since the emission spectra have been corrected from the instrument response. Finally, an extra factor  $\gamma$  must be included in the pre-exponential term of Eq. (3) when only a part of the emission spectra is used to calibrate the response of the optical sensor, as it will be discussed later.

For application purposes, it is important to define the quality of an optical sensor, which can be determined by its sensitivity  $S$  to temperature changes. This parameter is defined as the rate of

change of the ratio  $R$  with temperature and it allows the comparison of different optical temperature sensors<sup>9,10,22</sup>,

$$S = \frac{dR}{dT} = \frac{E_{ij}}{K_B T^2} \cdot \frac{g_i}{g_j} \cdot \frac{C_i(\nu) \beta_{ik} A_i h\nu_{ik}}{C_j(\nu) \beta_{jk} A_j h\nu_{jk}} e^{-\frac{E_{ij}}{K_B T}} = R \left( \frac{E_{ij}}{K_B T^2} \right) \quad (4)$$

On the other hand, when comparing different devices or procedures designed to determine the temperature it is necessary to use the relative sensitivity, which can be expressed as the rate of change that undergoes the parameter  $Q$  used to measure the temperature,

$$S_R = \frac{1}{Q} \left( \frac{dQ}{dT} \right) \quad (5)$$

where the  $Q$  parameter can refer to the lifetime, the energy shift, or any other sensitive parameter of the luminescence<sup>9,10</sup>.

The calibration of the optical sensor is performed using the experimental fluorescence intensity ratio values,  $R_{Exp}$ , obtained at different temperatures. These values are fitted to an exponential function  $R_{Exp} = C \cdot \exp(-D/T)$ , where  $C$  and  $D$  are adjustable parameters. It is worth noting that the calculated parameters can differ from those obtained theoretically using the Eq. (3), as it will be discussed later.

Finally, in the case of  $\text{Er}^{3+}$  ion, the small energy gap between the thermalized  $^2\text{H}_{11/2}$  and  $^4\text{S}_{3/2}$  emitting levels produces, in a larger or a lesser extent, an overlapping of the emissions bands, being necessary to establish a fitting procedure to determine the contribution of each level to the total integrated intensity, and hence, to obtain the  $R_{Exp}$  value at each temperature. This is a real problem in low point symmetry sites, like the orthorhombic  $\text{D}_2$  site of the  $\text{Er}^{3+}$  ions in the garnet structure, for which it is normal to find less emission peaks than the predicted number of transitions between Stark levels, i.e. 48 peaks for the  $^2\text{H}_{11/2}(6) \rightarrow ^4\text{I}_{15/2}(8)$  emission and 16 for the  $^4\text{S}_{3/2}(2) \rightarrow ^4\text{I}_{15/2}(8)$  one. This gives rise to a thermalized emission spectrum with many peaks that makes the process of deconvolution, in general, a difficult task. Despite of this drawback, two methods have been proposed by different authors to calculate the experimental value of the fluorescence intensity ratio in crystalline matrices<sup>23,24</sup>.

In the first method, two peaks associated with transitions between Stark levels of the thermalized and the ground states are selected, with the main criterion of changing more significantly with temperature than the other peaks<sup>23</sup>,

$$R_{Exp} = \frac{I_{Stark}^{2H_{11/2}}}{I_{Stark}^{4S_{3/2}}} \quad (6)$$

In the second method, the emission spectrum is divided in two parts, which correspond to the emission of all the Starks of each thermalized level to the ground state. In this case, the experimental ratio value  $R_{Exp}$  is equal to the ratio of the areas under the total emission profile of each part<sup>22,24</sup>,

$$R_{Exp} = \frac{I_{Area1}^{2H_{11/2}}}{I_{Area2}^{4S_{3/2}}} \quad (7)$$

Both methods have been used in this work to calibrate the temperature dependence of the  $\text{Er}^{3+}$  green emissions in YGG nano-garnets.

The calculation of the experimental values  $R_{\text{Exp}}$  requires mathematical software that allows the analysis of the emission spectrum. However, and thinking in a commercial prototype, this procedure is equivalent to use appropriate optical filters, in such a way that the current generated in the photodetector is proportional to the transmitted emission intensity. Thus, the intensity of each Stark level Eq. (6), can be obtained using bandpass filters (~5nm, for example). Meanwhile, the emission area of each level, Eq. (7), requires the use of broader bandpass filters or the combined use of short- and long-pass filters.

## C. Results and discussion.

### C.A. Absorption and luminescence at room temperature.

For any optical application it is important to know the local structure around the  $\text{RE}^{3+}$  ions inside the matrix, since it rules the fine structure splitting of the free-ion multiplets and the forced intra-configurational 4f-4f electric-dipole transition probabilities in the optical (UV-VIS-NIR) range. In the case of garnet structure, the  $\text{RE}^{3+}$  ions are expected to predominantly enter into the dodecahedral sites occupied by the  $\text{Y}^{3+}$  ions, being surrounded by eight oxygen ligands. As a result, the  $D_2$  crystal-field interaction causes a complete breakdown of the degeneracy of the electronic levels giving rise to  $(2J+1)/2$  Stark levels. This splitting can easily be identified from absorption, emission and excitation optical measurements<sup>19,22</sup>.

Room temperature diffuse reflectance spectrum, which is equivalent to the absorption one, of the YGG5Er sample was measured in the optical range (see **Figure 2**). In this spectrum, several bands corresponding to intra-configurational  $4f^{11}-4f^{11}$

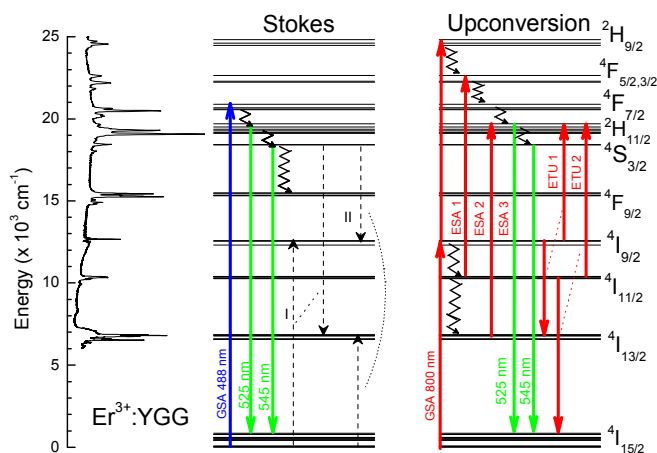
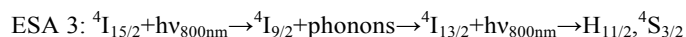
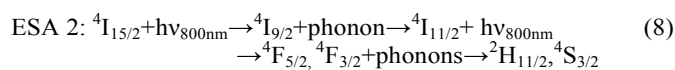
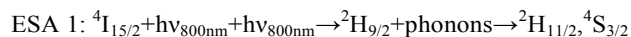


**Figure 2.** Diffuse reflectance spectrum of the YGG5Er nano-garnet and partial energy level diagram of the  $\text{Er}^{3+}$  ion. (Left) After a 488 nm ground state absorption (GSA, blue line), the multiphonon de-excitation channels (zig-zag lines) populate the thermalized levels, from which the Stokes green luminescence takes place (green lines), together with different cross-relaxation energy transfer processes (in dotted lines and roman numbers). (Right) After a 800 nm ground state absorption (GSA, red line), different excited state absorption ESA and energy transfer upconversion ETU mechanisms (red lines) are triggered to populate the thermalized levels, from which the upconverted green luminescence takes place (green lines)

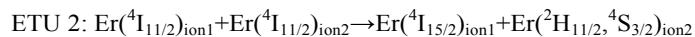
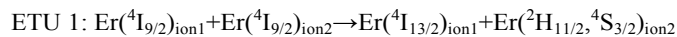
electronic transitions between the Stark levels of the  $^4I_{15/2}$  ground state and those of the different excited multiplets of the  $\text{Er}^{3+}$  ion are identified<sup>25</sup>. Transitions between multiplets have been labeled according to the well-known Dieke's diagram<sup>26</sup> and their origin is assumed to be electric-dipole in nature, except for the  $^4I_{13/2}$  first excited state that also shows a significant magnetic-dipole contribution. The sharp peak profiles found for all the electronic transitions confirm that the  $\text{Er}^{3+}$  ions are incorporated in the crystalline garnet structure of the nanoparticles.

Taking into account the diffuse reflectance spectrum and the energy level diagram, two different strategies can be used to obtain the green emissions of the  $\text{Er}^{3+}$  ions, which are originated by the  $^2H_{11/2}, ^4S_{3/2} \rightarrow ^4I_{15/2}$  radiative transitions from the thermalized levels to the ground state: The first one consists of exciting resonantly the  $\text{Er}^{3+}$  ions from the  $^4I_{15/2}$  ground state to the  $^4F_{7/2}$  level with a cw 488 nm blue laser radiation, followed by a fast non-radiative multiphonon relaxation to the thermalized emitting levels, which finally emit. The second strategy implies obtaining the green emissions by infrared-to-green energy upconversion processes triggered by a cw 800 nm laser radiation.

The processes involved in the latter strategy can be explained on the basis of two mechanisms: the excited state absorption (ESA) and the energy transfer upconversion (ETU). The first involves only one optically active ion successively promoted, within the time duration of the laser pulse (~5 ns), to the upper levels by the resonant absorption of two laser photons as follows<sup>19</sup> (see **Figure 2**):



The ETU processes are many-body mechanisms involving two or more nearby interacting optically active  $\text{Er}^{3+}$  ions. In this case, there must be two  $\text{Er}^{3+}$  ions in an intermediate excited level with a relatively long lifetime (reservoir metastable level), from which one  $\text{Er}^{3+}$  ion returns to the ground state (donor  $\text{Er}^{3+}$  ion) while the other  $\text{Er}^{3+}$  ion (acceptor  $\text{Er}^{3+}$  ion) is promoted up to the thermalized emitting levels. This mechanism is called cross-relaxation and the most resonant channels for the ETU are:



It is worth noting that both mechanisms are not mutually exclusive and can coexist to effectively contribute to the population of the excited emitting levels, although normally one of them dominates in the upconversion process. For  $\text{Er}^{3+}$  ions, these processes may be triggered by two excitation wavelengths, i.e. 800 nm and 980 nm, although the best efficiency is obtained exciting at 800 nm<sup>27,28</sup>.

Based on these processes, the green emissions of YGG01Er nano-garnet exciting in the blue at 488 nm and in the NIR at 800 nm have been measured and compared in **Figure 3**. The

main feature of both spectra is that they present identical luminescence profiles, a characteristic also observed in the other nano-garnets. This result can be understood if one takes into account that, under steady-state conditions, the emission from each thermalized level depends on its  $\text{Er}^{3+}$  population and the radiative probability of the transition involved, see Eq. (2), regarding that these parameters remain constant and independent of the laser excitation used.

However, this does not imply that the dynamics of the Stokes and the upconversion processes are the same neither for the same sample nor for the other nano-garnets with different  $\text{Er}^{3+}$  concentrations. To verify this, it is only necessary to study the dynamics of the luminescence decay curves under 488 and 800 nm pulsed laser excitations as a function of the  $\text{Er}^{3+}$  concentration.

Exciting at 488 nm the  $\text{Er}^{3+}$  ions immediately populate the  ${}^2\text{H}_{11/2}$ ,  ${}^4\text{S}_{3/2}$  thermalized levels, from which the spontaneous luminescence decay curves can be recorded. At very low concentrations of optically active ions, the interactions between them are negligible and the decay of the luminescence can be described by a single exponential. However, at higher

concentrations the active ions are closer to each other and the energy transfer processes become more efficient causing faster, non-exponential decays. For this reason, an effective lifetime ( $\tau_{\text{eff}}$ ) can be evaluated by using the following equation

$$\tau_{\text{eff}} = \frac{\int t \cdot I(t) \cdot dt}{\int I(t) \cdot dt} \quad (10)$$

The  $\tau_{\text{eff}}$  at room temperature (RT) of the  ${}^2\text{H}_{11/2}$  and  ${}^4\text{S}_{3/2}$  thermalized levels are found to be around 110, 100, and 45  $\mu\text{s}$  for the YGG01Er, YGG1Er, and YGG5Er nano-garnets, respectively (see upper inset in **Figure 3**). The green luminescence decay curve for the lowest  $\text{Er}^{3+}$  concentration is purely exponential, indicating a homogeneous distribution of active ions in the nanocrystals and, therefore, an  $\text{Er}^{3+}$ - $\text{Er}^{3+}$  distance large enough to, in a first approximation, neglect the energy transfer processes. At higher  $\text{Er}^{3+}$  concentrations, the observed non-exponential nature of the luminescence decays is accompanied by a shortening of the lifetime that is related to energy transfer processes between  $\text{Er}^{3+}$  ions and/or to different quenching traps, such as impurities and/or defective sites<sup>19</sup>. The resonant cross-relaxation channels that depopulate these thermalized levels are described by Eqs. (9) and shown in **Figure 2**.

On the other side, the temporal evolution of the upconverted green luminescence of the YGG nano-garnets is shown in the bottom inset of **Figure 3**. The intensity curves show a fast initial intensity rise from non-zero population, followed by a slight increase to a maximum and finally decrease. The non-zero population of the thermalized levels coincides in time with the pulsed laser excitation and is the fingerprint of the ESA processes, whereas the subsequent slow rise indicates that a second mechanism is feeding the emitting levels through ETU mechanisms<sup>19</sup>. Since the lifetime of the intermediate levels are involved in the process, the intensity of the upconverted emission reaches its maximum at around 10  $\mu\text{s}$  after the laser pulse for the three samples.

Finally, it is worth noting that, for both processes, a decrease of the experimental lifetime implies that a concentration quenching of the emission is taking place. Therefore, nano-garnets doped with a low concentration of optically active ions are more likely to produce luminescence transitions with higher quantum efficiencies.

### C.B. Temperature dependence of the Stokes $\text{Er}^{3+}$ luminescence.

In order to calibrate the  $\text{Er}^{3+}$ -doped YGG nano-garnets for optical temperature sensor applications, the behavior of the  ${}^2\text{H}_{11/2}$ ,  ${}^4\text{S}_{3/2} \rightarrow {}^4\text{I}_{15/2}$  green emissions have been measured in the temperature range from 300 to 800 K exciting with a 488 nm blue laser radiation. **Figure 4** shows the luminescence as a function of the temperature for the samples with the lowest (YGG01Er) and the highest (YGG5Er) concentrations of  $\text{Er}^{3+}$  ions, respectively, while the YGG1Er nano-garnets have an intermediate behavior (not shown). For all the samples, the  ${}^2\text{H}_{11/2} \rightarrow {}^4\text{I}_{15/2}$  emission intensity gradually increases with temperature at the expenses of the  ${}^4\text{S}_{3/2} \rightarrow {}^4\text{I}_{15/2}$  one, as expected from Eq. (3).

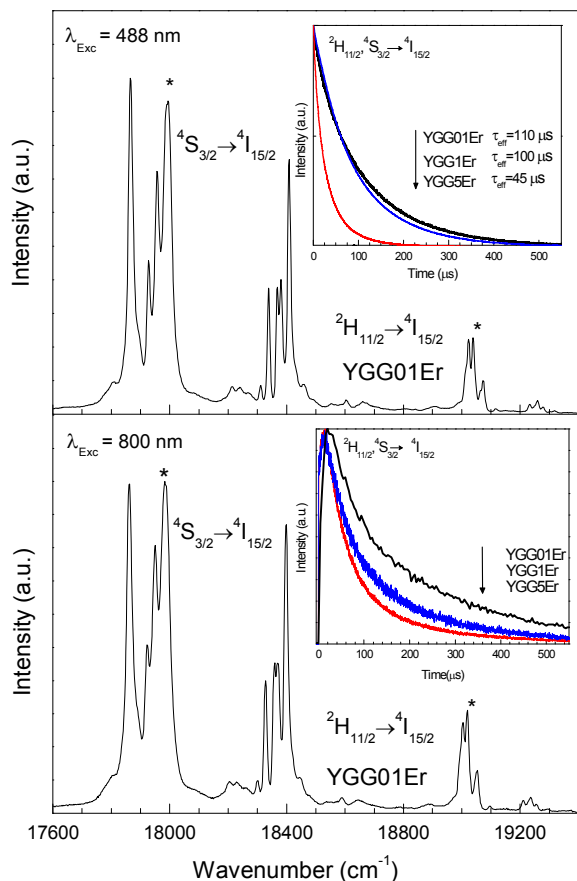


**Figure 3.** Green emissions of the YGG01Er nano-garnets obtained exciting with laser radiations at 488 nm (top) and at 800 nm (bottom). The asterisks (\*) indicate the Stark levels used to calculate the experimental fluorescence intensity ratio  $R_{\text{Exp}}$ . Insets show the dynamics of the green luminescence of the YGG nano-garnets for both laser excitations and different  $\text{Er}^{3+}$  concentrations.

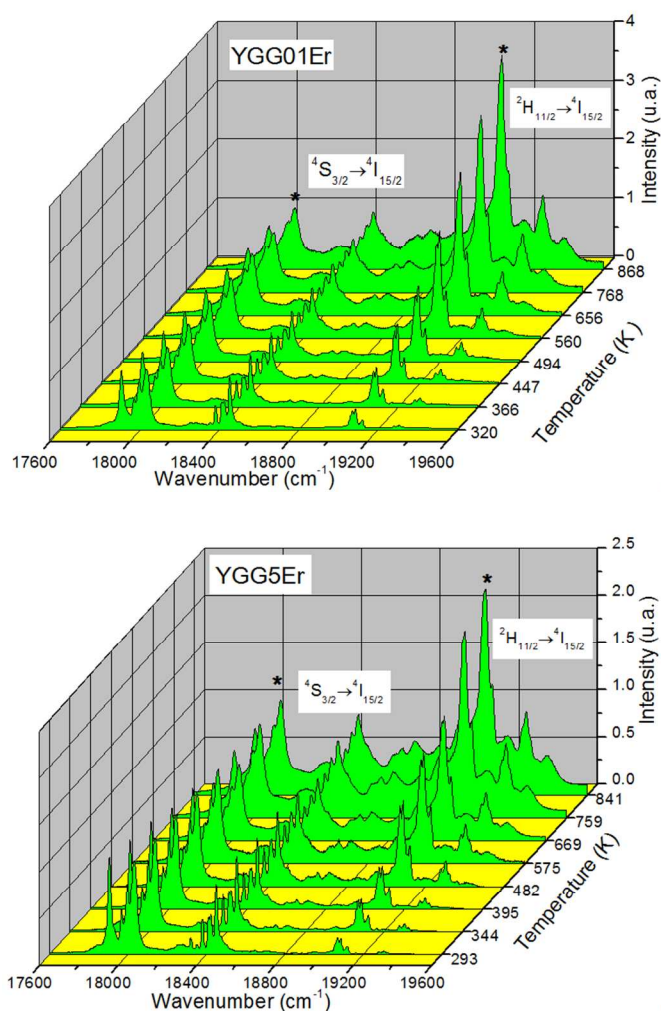


**Figure 4.** Temperature dependence of the  $\text{Er}^{3+}$  green emissions for the YGG01Er (top) and YGG5Er (bottom) nano-garnets. All the spectra are normalized to the maximum intensity of the  ${}^4\text{S}_{3/2} \rightarrow {}^4\text{I}_{15/2}$  transition.

This fact can be explained as the increase of the population of the upper thermalized level with temperature according to the Boltzmann distribution. However, and despite that the  $\text{Er}^{3+}$  ion population increases with an exponential behavior for all the samples, the emission intensity of the  ${}^2\text{H}_{11/2} \rightarrow {}^4\text{I}_{15/2}$  band does not vary with the same rate for all the  $\text{Er}^{3+}$  concentrations, being much faster for the lowest  $\text{Er}^{3+}$ -doped nano-garnet. This effect is clearly observed in more detail in the green emissions of the three  $\text{Er}^{3+}$ -doped YGG nano-garnets studied at RT, and shown in **Figure 5**, in which all the spectra have been normalized to the maximum of the  ${}^4\text{S}_{3/2} \rightarrow {}^4\text{I}_{15/2}$  emission. When the doping concentration increases the emission intensity of the  ${}^2\text{H}_{11/2} \rightarrow {}^4\text{I}_{15/2}$  transition decreases, whereas the changes in the  ${}^4\text{S}_{3/2} \rightarrow {}^4\text{I}_{15/2}$  emission band seem to be less important. These results clearly point to microscopic processes related to the concentration of  $\text{Er}^{3+}$  ions in the nano-garnet, i.e. the energy transfer processes between  $\text{Er}^{3+}$  ions. Actually, this effect can be related to re-absorption processes inside the nanoparticles, which are quite common for the  $\text{Er}^{3+}$  in solid matrices<sup>22,29</sup>. The reabsorption is a process in which a photon emitted by an  $\text{Er}^{3+}$  ion is absorbed before leaving the sample by other  $\text{Er}^{3+}$  ions, which are not being directly excited by the laser. To

observe this phenomena three conditions must be satisfied simultaneously: first, the concentration of  $\text{Er}^{3+}$  ion should be large enough to guarantee an effective absorption by non-excited  $\text{Er}^{3+}$  ions in the path followed by the emitted photons inside the matrix; second, there must be a large overlap between the emission and absorption bands of the  $\text{Er}^{3+}$  ions involved; and third, the oscillator strengths of the transitions involved should be large. That is why the effects of the energy transfer between  $\text{Er}^{3+}$  ions, enhanced with the optically active ion concentration, are more important for transitions involving the  ${}^2\text{H}_{11/2}$  upper level, since the  ${}^4\text{I}_{15/2} \rightarrow {}^2\text{H}_{11/2}$  absorption peak has a relatively large oscillator strength (see the normalized diffuse reflectance spectrum in **Figure 5**).

The physical process of the re-absorption is a sort of radiative energy transfer involving real photons that for nanoparticles could be explained as follows: when the laser reaches the surface of the pellet, the high scattering of these nanoparticles would allow effectively propagating the laser beam only a few hundreds of micrometers inside it. The green photons collected by the detecting lens come from the laser pumped volume. However, when the laser pumped volume is located inside the sample, the green photons collected by the detecting lens system come from two different sources: first, those emitted by the  $\text{Er}^{3+}$  ions directly excited by the laser after crossing a portion of the sample; and second, green photons re-emitted after the re-absorption of some of the previous photons by other  $\text{Er}^{3+}$  ions located on the way out of the sample, and following a ( ${}^2\text{H}_{11/2} \rightarrow {}^4\text{S}_{3/2}$ ;  ${}^4\text{I}_{15/2} \rightarrow {}^4\text{I}_{15/2}$ ;  ${}^2\text{H}_{11/2} \rightarrow {}^4\text{S}_{3/2}$ ) cross-relaxation scheme.

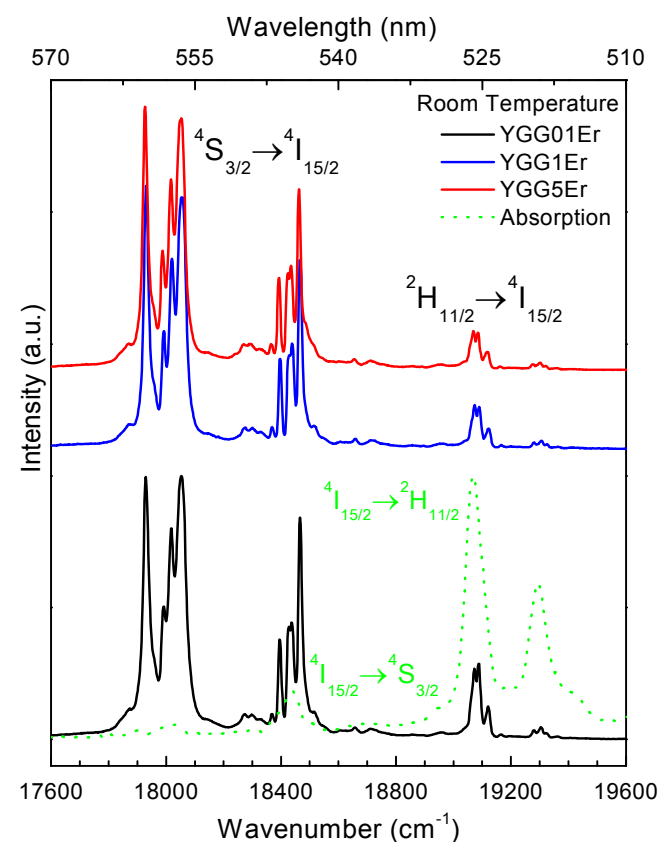


**Figure 5.** Room temperature green emissions (solid line) of  $\text{Er}^{3+}$ -doped YGG nano-garnets after a cw 488 nm laser excitation. The normalized diffuse reflectance spectrum (dotted line) associated with the  ${}^4\text{I}_{15/2} \leftrightarrow {}^4\text{S}_{3/2}$ ,  ${}^2\text{H}_{11/2}$  transitions are also included for comparison.

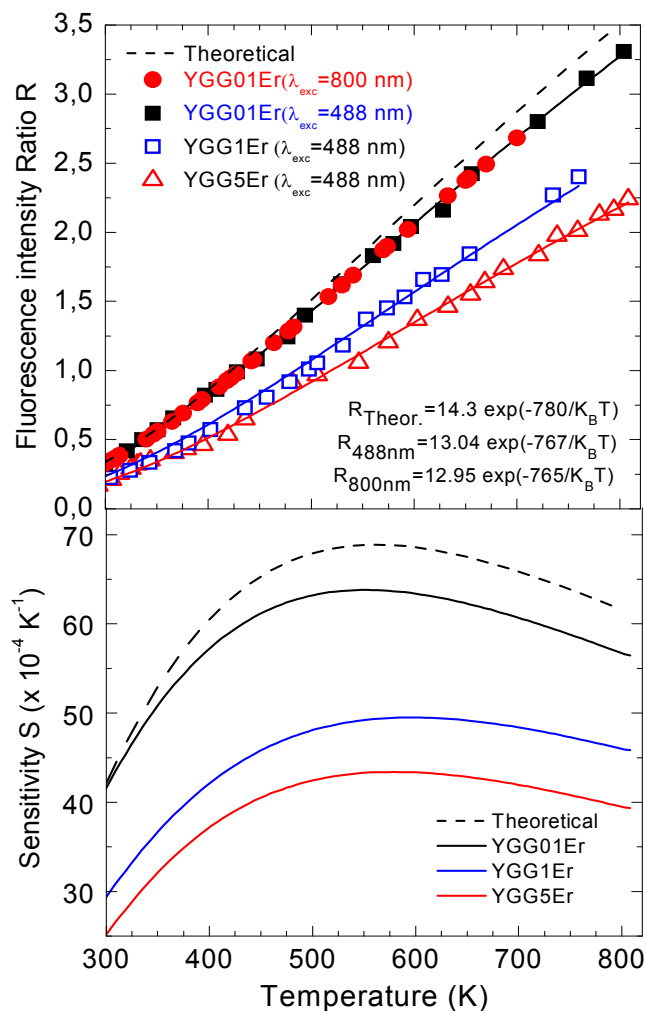


**Figure 6.** Theoretical and experimental “Stark” fluorescence intensity ratios and thermal sensitivities of the YGG nano-garnets doped with different  $\text{Er}^{3+}$  concentrations in the range from 300 to 800 K under blue and NIR laser excitations. The experimental R values have been fitted to Eq. (6) (in solid lines).

Since the spontaneous re-emission is produced in all direction, it gives rise to an effective decrease in the number of green photons in the solid angle of the detection system, hence producing a lower emission intensity of the  ${}^2\text{H}_{11/2} \rightarrow {}^4\text{I}_{15/2}$  transition and, therefore, a lower value for the experimental intensity ratio  $R_{\text{exp}}$  with the  $\text{Er}^{3+}$  concentration. From the point of view of the analysis of the energy transfer processes, individually each YGG nanoparticle can be considered as a bulk matrix, since the range of sizes allows assuming that re-absorption is taking place inside each nanoparticle. However, there could be also radiative re-absorption between the different layers of YGG nano-garnets, keeping in mind the high scattering of light produced by these nanoparticles.

Since the emissions spectra present a strong dependence with the concentration of  $\text{Er}^{3+}$  ions, therefore the fluorescence intensity ratio technique should also show this behavior. **Figure 6** shows the experimental intensity ratio calculated from the Stark ratio method, Eq. (6), for the three  $\text{Er}^{3+}$  concentrations as a function of the temperature.

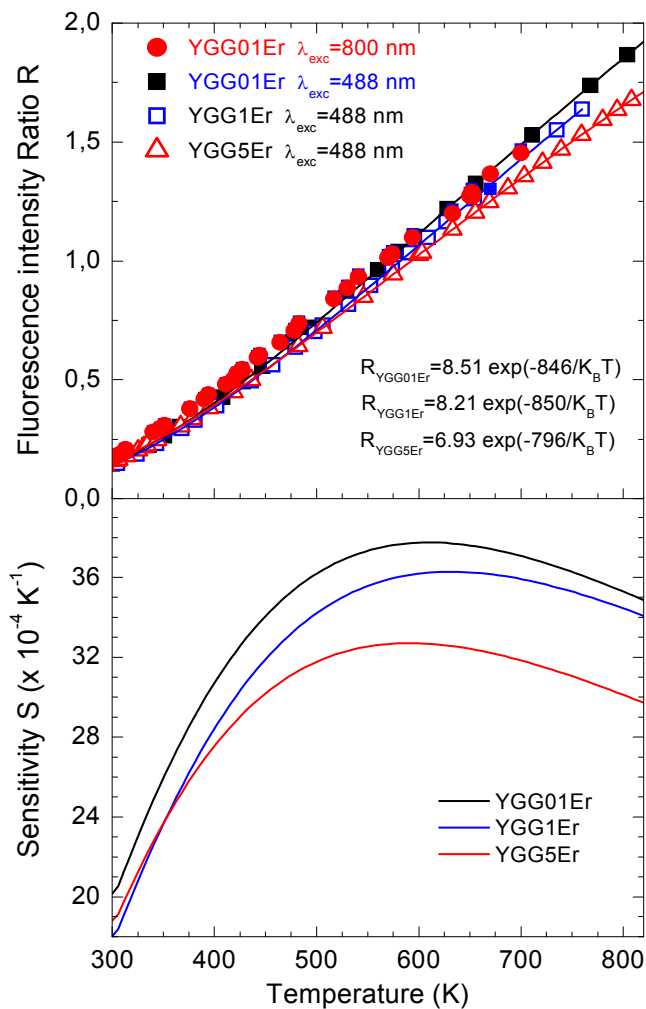


**Figure 7.** Experimental “Area” fluorescence intensity ratios and thermal sensitivities for the YGG nano-garnets doped with different  $\text{Er}^{3+}$  concentrations in the range from 300 to 800 K under blue and NIR laser excitations. The experimental R values have been fitted to Eq. (7) (in solid lines).

The peaks between Stark levels selected for both emissions are indicated with asterisks in **Figures 3** and **4**. On the other side, these results can be compared with those using the total areas of both emission bands, calculated the areas between 17500 to 18575  $\text{cm}^{-1}$  for the  ${}^2\text{H}_{11/2} \rightarrow {}^4\text{I}_{15/2}$  transition and from 18575 to 19920  $\text{cm}^{-1}$  for the  ${}^4\text{S}_{3/2} \rightarrow {}^4\text{I}_{15/2}$  transition and using Eq. (7) (see **Figure 7**). All the experimental values have been fitted to an exponential function, similar to Eq. (3), and the fitted coefficients are given in the **Table 1** for both methods.

For all the nano-garnets, the calculated values of the energy gap are similar than that obtained from the diffuse reflectance spectrum, finding the most important difference in the pre-exponential factor, which changes from 9.28 to 13.4 using Eq. (6), and from 6.93 to 8.51 using Eq. (7). For both methods, the pre-exponential factor increases with the decrease of the  $\text{Er}^{3+}$  concentration, with a higher rate for the Stark ratio method, confirming that this coefficient reflects more significantly the negative effect of the re-absorption. Moreover,

**Table 1.** Values for the pre-exponential factor, the energy gap between the thermalized levels, and the maximum sensitivity as a function of the Er<sup>3+</sup> concentration [see Eq. (3) and (4)].

YGG nano-garnets	Pre-exponential Factor	E <sub>32</sub> (cm <sup>-1</sup> )	Maximum sensitivity S (10 <sup>-4</sup> K <sup>-1</sup> ) at T <sub>max</sub>	T <sub>max</sub> (K)
Theoretical	14.30	750	71	540
Stark ratio				
YGG01Er	13.04	767	64	547
YGG1Er	10.36	786	50	594
YGG5Er	9.28	802	43	569
Area ratio				
YGG01Er	8.51	846	37	610
YGG1Er	8.21	850	36	632
YGG5Er	6.93	796	33	592

the thermal sensitivity of each sample, calculated with Eq. (4), has been also included in **Figures 6** and **7**. Results indicate that using the ratio of intensities of individual peaks between Stark levels (the Stark ratio method) allows obtaining a calibration with a better response and sensitivity to temperature changes of the nano-garnets, due to the high temperature sensitivity of their intensities.

These experimental calculations can be compared with the theoretical intensity ratio R<sub>Theor</sub> for the green emissions of the YGG nano-garnets. Using Eq. (3) it is only necessary to give the values for the energy gap, the radiative probabilities, the degeneracies of the thermalized levels and the average photon energy. For this purpose, the values for energy gap and the average energy photons emitted are estimated directly from the diffuse reflectance spectrum (see **Figure 2**). In contrast, the radiative probabilities are calculated from the Judd-Ofelt parameters (Ω<sub>2</sub>, Ω<sub>4</sub>, Ω<sub>6</sub>)<sup>30,31</sup> and the double-reduced matrices given by Carnall *et al.*<sup>32</sup>, which for the thermalized levels of the Er<sup>3+</sup> ions can be expressed as

$$\begin{aligned}
 A(^2H_{11/2} \rightarrow ^4I_{15/2}) &\propto 0.7158 \cdot \Omega_2 + 0.4138 \cdot \Omega_4 + 0.0927 \cdot \Omega_6 \\
 A(^4S_{3/2} \rightarrow ^4I_{15/2}) &\propto 0.2225 \cdot \Omega_6
 \end{aligned}
 \quad (11)$$

In bulk matrices, the Judd-Ofelt parameters are estimated from the least square fit between the experimental and theoretical oscillator strengths<sup>30,31,33</sup>. Nevertheless, this method cannot be used for the nano-garnets under study since the powder is not transparent and only the diffuse reflectance can be measured. Therefore, we can only obtain a relative measurement of the absorption in the matrix. However, in the literature one can find examples in which the experimental lifetimes for an electronic level of a RE<sup>3+</sup> ion introduced as dopant in a bulk matrix and its equivalent nanoparticle have been compared, and the radiative probabilities have been considered approximately equal<sup>34,35</sup>. For example, Lipińska *et al.*<sup>34</sup> have calculated the lifetime of the <sup>4</sup>F<sub>3/2</sub> level of Nd<sup>3+</sup> ions in Gd<sub>3</sub>Ga<sub>5</sub>O<sub>12</sub> (GGG) nanopowder and crystal garnets, and they found comparable results between them, or V. I. Zhekov *et al.*<sup>35</sup> in Y<sub>3</sub>Al<sub>5</sub>O<sub>12</sub> (YAG) crystal doped with Er<sup>3+</sup> ions have observed a similar behavior for the <sup>4</sup>I<sub>13/2</sub> → <sup>4</sup>I<sub>15/2</sub> transition. Although it has not been possible to find previous studies for YGG crystal bulk, Sardar *et al.*<sup>36</sup> have

calculated the Judd-Ofelt parameters and the radiative probabilities for different Er<sup>3+</sup>-doped garnets (Y<sub>3</sub>Al<sub>5</sub>O<sub>12</sub>, Y<sub>3</sub>Sc<sub>2</sub>Ga<sub>3</sub>O<sub>12</sub> y Gd<sub>3</sub>Ga<sub>5</sub>O<sub>12</sub>) with a similar composition to the Y<sub>3</sub>Ga<sub>5</sub>O<sub>12</sub> sample under study. Assuming that replacing Yttrium for Gadolinium does not change the radiative probabilities to a larger extend and that the Judd-Ofelt parameters for YGG crystal and nanoparticles are similar, it is possible to make an estimation of the radiative probabilities of the <sup>2</sup>H<sub>11/2</sub> and <sup>4</sup>S<sub>3/2</sub> levels from of the values reported for GGG crystal (Ω<sub>2</sub>=0.70, Ω<sub>4</sub>=0.37, Ω<sub>6</sub>=0.86, x 10<sup>-20</sup> cm<sup>2</sup>)<sup>36</sup>. This allows obtaining a theoretical intensity ratio equal to 4.5·exp(-750/K<sub>B</sub>T).

When this theoretical result is compared to the experimental expressions obtained from fluorescence intensity ratios between Stark levels a large difference between them is observed. This difference appears because, by definition, the theoretical pre-exponential factor represents the ratio between the total emission of each level [see Eqs. (2) and (3)]. However, in the experimental calculation, the ratio between the Stark peaks selected (indicated with an asterisk in **Figures 3** and **4**) has been only taken into account. To correct this fact, an extra parameter γ must be introduced in the Eq. (3), which indicates the percentage of the emission between Stark levels considered respect to the total emission of each multiplet. These percentages have been calculated as follows

$$\begin{aligned}
 \gamma^2 H_{11/2} &= \frac{\text{Area}_{\text{Stark selected}}^{2H_{11/2} \rightarrow ^4I_{15/2}}}{\text{Area}_{\text{Total emission}}^{2H_{11/2} \rightarrow ^4I_{15/2}}} \\
 \gamma^4 S_{3/2} &= \frac{\text{Area}_{\text{Stark selected}}^{4S_{3/2} \rightarrow ^4I_{15/2}}}{\text{Area}_{\text{Total emission}}^{4S_{3/2} \rightarrow ^4I_{15/2}}}
 \end{aligned}
 \quad (12)$$

When these percentages are introduced in Eq. (3), the theoretical intensity ratio of the green emissions is equal to 14.3·exp(-750/K<sub>B</sub>T), a result much closer to the experimental 13.04·exp(-767/K<sub>B</sub>T) obtained for the nano-garnet with the lowest Er<sup>3+</sup> concentration.

### C.C. Temperature dependence of the upconverted Er<sup>3+</sup> luminescence.

After finding the dependency between the Er<sup>3+</sup> ions concentration and the thermal sensitivity of the optical sensor, this section examined whether the use of other laser excitation wavelengths, which triggers different mechanisms and processes to obtain the thermalized green luminescence, also affects the thermal sensitivity. The blue laser involves a linear process with the pump power (I<sub>em</sub> ∝ I<sub>pump</sub>), while the second is non-linear (I<sub>em</sub> ∝ I<sub>pump</sub><sup>n</sup>), where n represents the number of quantum energies of the exciting photon needed to obtain the green upconverted emission. For this study the sample with the lowest Er<sup>3+</sup> concentration, and therefore with the highest sensitivity, was selected.

The green upconverted emissions of the YGG01Er nano-garnet were measured in the temperature range of 300 to 700 K exciting with a cw 800 nm NIR laser radiation in the same optical setup than for the other experiment (see **Figure 1**). The experimental values for the fluorescence intensity ratio of the Stokes and green upconverted emissions using both methods are compared in **Figure 6** and **7**. The experimental calibration obtained using the upconverted emission intensities is exactly

the same, within the experimental errors, to that found for the Stokes luminescence exciting the sample with a blue 488 nm laser. Therefore, when these are fitted to an exponential function, similar to Eq. (3), the coefficients do not change significantly. The small differences between them can be justified if one considers that the distribution of the experimental data and the temperature range are not exactly equal, and may affect in the least squares fitting procedure. Thus, as already mentioned, the possibility to obtain the same luminescence using different excitation wavelengths increase the number of applications for which these nano-sensors can be employed. Especially in medicine, since the human skin is transparent to the 800 nm NIR radiation.

### C.D. YGG nanocrystalline garnet as biological optical temperature sensor.

It is known that in any biological system the temperature plays a crucial role in its dynamics, i.e. in the rate of cell division<sup>37,38</sup>. The use of the YGG nano-garnets as temperature nano-sensors in biological systems has the disadvantage that they must be functionalized before being introduced in aqueous media, in order to avoid the luminescence inhibition by the presence of OH-groups that interact with the optically active ions<sup>39</sup>. This disadvantage is solved if the nano-garnets are coated with an insulating material, i.e. a silica shell, preventing the transfer of energy from the optically active RE<sup>3+</sup> ions to these impurities that generates channel of luminescence losses<sup>38</sup>. In this work, the Er<sup>3+</sup>-doped YGG nano-garnets were calibrated without the presence of this isolating material and, therefore they were not dissolved in any liquid. The experimental setup used is the same that for the previous studies (see **Figure 1**), and only the YGG01Er nano-garnet was analyzed.

The luminescence temperature dependence of this sample is given in **Figure 8**, where only a part of the emission of the  $^4S_{3/2} \rightarrow ^4I_{15/2}$  is represented to show more clearly the changes of the  $^2H_{11/2} \rightarrow ^4I_{15/2}$  band in the biological range from 292 K (19 °C) to 335 K (62 °C). The inset in **Figure 8** shows the

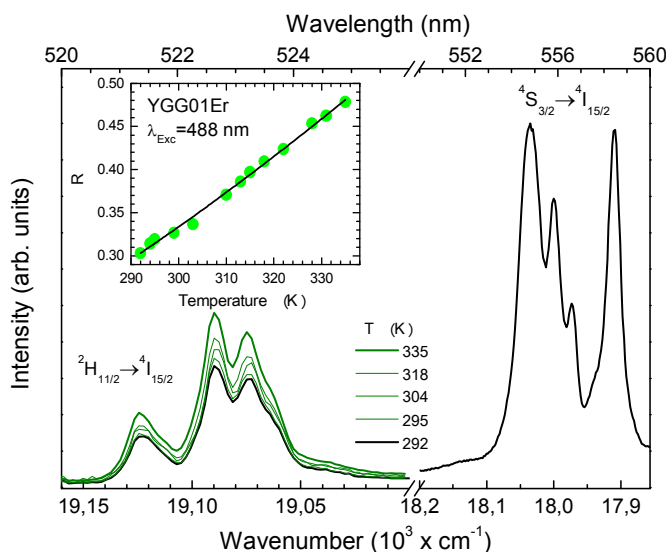


**Figure 8.** Temperature dependence of the Er<sup>3+</sup> green emissions for the YGG01Er nano-garnet in the biological range from 292 to 335 K (19 to 62 °C). The inset shows the fluorescence intensity ratio and the fit to single exponential.

experimental non-linear calibration curve, which is equal to  $11.04 \cdot \exp(-728/K_B T)$ . The difference between these values and the previous calibration is justified by the short temperature range studied and the data distribution. In addition, these coefficients are similar to the theoretical curve,  $14.3 \cdot \exp(-750/K_B T)$ .

Finally, the thermal sensitivity of the YGG nano-garnets is compared in **Table 2** with other samples that have been also proposed as nano-sensors to measure the temperature in biological systems. For this purpose, the relative sensitivity of these devices have been calculated according to Eq. (5). As shown, the YGG nano-garnets present a relative sensitivity similar than the other samples proposed, confirming that they are excellent temperature sensors to be used in biological and biomedical applications.

**Table 2.** Relative sensitivity in the biological range from 292 to 335 K (19 to 62 °C) of different Er<sup>3+</sup>-optical temperature sensors proposed in the literature. All of them are based on the fluorescence intensity ratio of the green emissions of the Er<sup>3+</sup> ions.

Host	Relative sensitivity at 335 K $S_R$ ( $\times 10^{-4} K^{-1}$ )	Reference
YGG Nano-garnets	45	This work
Silicate (glass)	21	[40]
Ga <sub>2</sub> S <sub>3</sub> :La <sub>2</sub> O <sub>3</sub> (glass)	19	[41]
Gd <sub>2</sub> O <sub>3</sub> (nanoparticles)	12	[42]
NAYF <sub>4</sub> (Microsphere)	9	[2]
Phosphate (glass)	5	[43]

### Conclusions.

Y<sub>3</sub>Ga<sub>5</sub>O<sub>12</sub> garnet nanoparticles with typical sizes ranging from 40 to 60 nm and doped with different concentrations of Er<sup>3+</sup> ions have been synthesized by the conventional citric acid sol-gel Pechini method. The Stokes and upconverted Er<sup>3+</sup> green luminescence can be obtained exciting with a 488 nm blue laser and an 800 nm near-infrared laser, respectively, despite their dynamics are totally different. For both laser excitations, the temperature dependent  $^2H_{11/2}, ^4S_{3/2} \rightarrow ^4I_{15/2}$  thermalized green emissions have been calibrated using the fluorescence intensity ratio technique in the temperature range from 300 to 850 K. The results show that the emission associated with the  $^2H_{11/2} \rightarrow ^4I_{15/2}$  transition increases its intensity compared to the  $^4S_{3/2} \rightarrow ^4I_{15/2}$  transition when the temperature increases following a Boltzmann distribution of the Er<sup>3+</sup> populations between the  $^2H_{11/2}, ^4S_{3/2}$  thermalized levels. However, it has been observed that the rate of this increase depends on the Er<sup>3+</sup> ion concentration, being more intense for low dopant concentrations. In fact, the sensitivity to temperature changes of the lowest doped YGG nanoparticles is twice as large as that for the most doped sample. Due to this excellent result, a careful calibration in the biological range has been carried out and, in larger detail, from 292 to 335 K. The results suggest that Y<sub>3</sub>Ga<sub>5</sub>O<sub>12</sub> nanoparticles doped with the lowest Er<sup>3+</sup> concentration can be used in biological applications. Finally, it

has been shown that the behavior of the green luminescence with the temperature is independent of the laser excitation wavelength, blue or near-infrared, used, although the latter is more suitable for biomedical applications.

### Acknowledgements.

This work have been partially supported by Ministerio de Economía y Competitividad de España (MINECO) under The National Program of Materials (MAT2010-21270-C04-02/-03, and MAT2013-46649-C4-3-P/-4-P), The Consolider-Ingenio 2010 Program (MALTA CSD2007-00045), and the Indo-Spanish Joint Programme of Cooperation in Science and Technology (PRI-PIBIN-2011-1153/DST-INT-Spain-P-38-11), and by the EU-FEDER funds. V. Venkatramu is also grateful to Council of Scientific and Industrial Research (CSIR), New Delhi for the sanction of major research project (No. 03(1229)/12/EMR-II, dated: 16th April, 2012). V. Monteseguro wishes to thank MICINN for the FPI grant (BES-2011-044596).

### Notes and references.

<sup>a</sup> Department of Physics, and MALTA Consolider Team, Universidad de La Laguna. 38200 San Cristóbal de la Laguna, Santa Cruz de Tenerife, Spain.

\* E-mail: sleonlui@ull.es (Dr. Sergio Fabián León Luis)

<sup>b</sup> Institute of Materials and Nanotechnology, Universidad de La Laguna. 38200 San Cristóbal de la Laguna, Santa Cruz de Tenerife, Spain.

<sup>c</sup> Department of Physics, Yogi Vemana University, Kadapa 516 003, India.

<sup>d</sup> Department of Applied Physics, and MALTA Consolider Team, Universidad de Cantabria. 39005 Santander, Cantabria, Spain.

<sup>e</sup> Institute of Advanced Studies in Atomic, Molecular and Photonics, Universidad de La Laguna. 38200 San Cristóbal de la Laguna, Santa Cruz de Tenerife, Spain.

- R. E. Bently, Handbook of Temperature Measurement, (1998) Springer.
- F. Vetrone, R. Naccache, A. Zamorrón, A. J. de la Fuente, F. Sanz-Rodríguez, L. M. Maestro, E. M. Rodríguez, D. Jaque, J. García-Solé, and J. A. Capobianco, ACS Nano 4 (2010) 3254-3258.
- E. Saïdi, N. Babinet, L. Lalouat, J. Lesueur, L. Aigouy, S. Volz, J. Labéguerie, and M. Mortier, Small 7 (2011) 259-264.
- X. Huang, P. K. Jain, I. H. El-Sayed, and M. A. El-Sayed, Photochemistry and Photobiology 82 (2006) 412-417.
- M. Johannsen, U. Gneveckow, B. Thiesen, K. Taymooiran, C. H. Cho, N. Waldöfner, R. Scholz, A. Jordan, S. A. Loening, and P. Wust, European Urology 52 (2007) 1653-1662.
- D. Jaque, and F. Vetrone, Nanoscale 4 (2012) 4301-4326.
- S. Ghaderi, B. Ramesh, and A. M. Seifalion, Journal of Drug Targeting 19 (2011) 475-486.
- S. A. Wade, Thesis: Temperature measurement using rare earth doped fiber fluorescence, 2003. Victoria University. Australia.
- S. A. Wade, S. F. Collins, and G. W. Baxter, Journal of Applied Physics 94 (2003) 4743-4756.
- V. K. Rai, Applied Physics B 88 (2007) 297-303.
- U. R. Rodríguez-Mendoza, E. A. Lalla, J. M. Cáceres, F. Rivera-López, S. F. León-Luis, and V. Lavín, Journal of Luminescence 131 (2011) 1239-1248.
- F. Ramos-Lara, D. Jaque, J. García-Solé, and U. Caldiño, Journal of Physics: Condensed Matter 12 (2000) L441-L449.
- X. Cheng, J. Collins, B. DiBartolo, B. Bowlby, B. Dinerman, and D. Weyburne, Journal of Luminescence 72-74 (1997) 168-170.
- L. M. Maestro, P. Haro-González, M. C. Iglesias-De La Cruz, F. Sanz-Rodríguez, Á. Juaranz, J. G. Solé, and D. Jaque, Nanomedicine 8 (2013) 378-379.
- M. Frede, R. Wilhelm, M. Brendel, C. Fallnich, F. Seifert, B. Willke, and K. Danzmann, Optics Express 12 (2004) 3581-3589.
- Yu. K. Voronko, A. A. Sobol, A. Ya. Karasik, N. A. Eskov, P. A. Rabochkina, and S. N. Usharov, Optical Materials 20 (2002) 197-199.
- V. Lupei, Optical Materials 19 (2002) 95-107.
- A. Benayas, D. Jaque, C. Jacinto, and A. A. Kaminskii, IEEE journal of Quantum Electronics 46 (2010) 1870-1876.
- V. Venkatramu, S. F. León-Luis, U. R. Rodríguez-Mendoza, V. Monteseguro, F. J. Manjón, A. D. Lozano-Gorrín, R. Valiente, D. Navarro-Urrios, C. K. Jayasankar, A. Muñoz, and V. Lavín, Journal of Materials Chemistry 22 (2012) 13788-13799.
- V. Monteseguro, P. Rodríguez-Hernández, V. Lavín, F. J. Manjón, and A. Muñoz, Journal Applied Physics 113 (2013) 183505 (7 pp).
- V. Monteseguro, P. Rodríguez-Hernández, R. Vilaplana, F. J. Manjón, V. Venkatramu, D. Errandonea, V. Lavín, and A. Muñoz, Journal of Physical Chemistry C 118 (2014) 13177-13185.
- S. F. León-Luis, U. R. Rodríguez-Mendoza, I. R. Martín, E. Lalla, and V. Lavín, Sensors and Actuators B: Chemical 176 (2013) 1167-1175.
- E. Maurice, G. Monnom, D. B. Ostrowsky, and W. Baxter, Journal of Lightwave Technology 13 (1995) 1349-1353.
- V. López, G. Paez, and M. Strojnik, Infrared Physics & Technology 46 (2004) 133-139.
- C. A. Morrison, and R. P. Leavitt, Spectroscopic properties of triply ionized lanthanides in transparent host crystals, in Handbook of the Physics and Chemistry of Rare Earths, edited by K. A. Gschneidner, Jr. and L. Eyring, North Holland Publishing Company, Vol. 5, Ch. 46, pp. 461-701.
- G. H. Dieke, Spectra and Energy levels of Rare-Earth Ions in Crystal, Wiley-Interscience, New York, 1968.
- F. Kaczmarek, Z. Stryla, and A. Jendzejczak, Applied Physics B: Laser and Optics 73 (2001) 125-128.
- K.W. Krämer, H. U. Güdel and R. N. Schwartz, Journal of Alloys and Compound 275-277 (1998) 191-195.
- C. Pérez-Rodríguez, L. L. Martín, S. F. León-Luis, K. K. Kumar, and C. K. Jayasankar, Sensors and Actuators B: Chemical 195 (2014) 324-331.
- B. R. Judd, Physical Review 127 (1962) 750-761.
- G. S. Ofelt, Journal Chemical Physics 37 (1962) 511-521.
- W. T. Carnall, G. L. Goodman, K. Rajnak, and S. R. Rana, Journal of Chemical Physics 90 (1989) 3443-3457.

- 33 S. F. León-Luis, U. R. Rodríguez-Mendoza, P. Haro-González, I. R. Martín and V. Lavín, *Sensors and Actuators B: Chemical* 174 (2012) 176-186.
- 34 L. Lipińska, W. Ryba-Romanowki, D. Rzepka, S. Ganschow, R. Lisiecki, R. Diduszko, and A. Pajączkowska, *Crystal Research and Technology* 44 (2009) 477-483.
- 35 V. I. Zhekov, T. M. Murina, A. M. Prokhorov, M. J. Studenikin, S. Georgescu, V. Lupci, and I. Ursu, *Soviet Journal of Quantum Electronics* 16 (1986) 274-276.
- 36 D. K. Sardar, W. M. Bradley, J. J. Perez, J. B. Gruber, B. Zandi, J. A. Mutchison, C. W. Trussell, and M. R. Kokta, *Journal of Applied Physics* 93 (2003) 2602-2607.
- 37 N. Barekzi, and M. Laroussi, *Plasma Processes and Polymers* 10 (2013) 1039-1050.
- 38 C. Theriault, E. Paetzell, R. Chandrasekar, C. Barkey, Y. Oni, and W.O. Soboyejo, *Materials Science and Engineering C* 32 (2012) 2242-2249.
- 39 C. Jeffrey Brinker, and G.W. Scherer, *Sol-Gel Science: The Physics and Chemistry of Sol-Gel Processing*, Academic Press Inc. (1990).
- 40 C. R. Li, B. Dong, S. F. Li, and C. L. Song: *Chemical Physics Letters* 443 (2007) 426-429.
- 41 P. V. dos Santos, M. T. de Araujo, A. S. Gouveia-Neto, J. A. M. Neto, and A. S. B. Sombra: *Applied Physics Letters* 73 (1998) 578-580.
- 42 S. K. Singh, K. Kumar, and S. B. Rai: *Sensors & Actuators A: Physical* 149 (2009) 16-20.
- 43 X. C. Yu, F. Song, C. G. Zou, L. J. Luo, C. G. Ming, W. T. Wang, Z. Z. Cheng, L. Han, T. Q. Sun, and J. G. Tian: *Optical Materials* 31 (2009) 1645-1649.